

# Stationary textures induced by spin-transfer torques: role of the angular dependence

Alejandro O. León

E-mail: aoleon@dfi.uchile.cl

Departamento de Física, Facultad de Ciencias Físicas y Matemáticas, Universidad de Chile, Casilla 487-3, Santiago, Chile.

**Abstract.** Magnetic systems forced with external fields or electric currents exhibit a rich spatiotemporal dynamics. A well known example is the one of spin-transfer torque driven textures, which includes switching, precessions, dissipative solitons, and periodic textures. Using different expressions that model the spin-transfer torque —angular dependence of the spin-transfer— we obtain analytic solutions for static spatially periodic states, study their stability, and elucidate the role that the angular dependence plays in the formation of textures. We demonstrate that the type of bifurcations changes from supercritical to subcritical, depending on the particular type of torque. Numerical simulations confirm this scenario. Thus, magnetoresistance measurements could permit to determine the form of the torque.

## 1. Introduction

Ferromagnetic materials subjected to dissipation and injection of energy or momentum self-organize in dissipative structures, such as solitons, skyrmions, periodic textures, and domain walls. The usual driving mechanisms are the couplings between the magnetization of the ferromagnetic material and external magnetic fields and electric currents. In 1996, Slonczewski [1] and Berger [2] predicted that a spin-polarized (SP) electric current exerts a torque in ferromagnetic nano-layers, effect known as spin-transfer torque [3, 4, 5]. Since then, the interest on excitations driven by SP currents has grown considerably, both from the scientific and the technological viewpoints [4]. A typical configuration to study spin-transfer torques is the multilayer nanopillar, or spin-valve, that consists on ferromagnetic conducting films separated by non-magnetic conductors as shown in Fig. 1(a). When an electric current is applied, it transfers spin angular momentum from one relatively thick layer with *fixed* magnetization to a thin film with *free* magnetization [4].

Spin-transfer torques are non-conservative effects, and therefore they can destroy, stabilize or destabilize states. Moreover, in the case in which a SP current injects enough energy to counterbalance the dissipation, the free magnetization switches or precesses with microwave frequencies, both effects have been studied experimentally [6, 7, 8, 9] and theoretically [10, 11, 12, 13]. Hence, electric currents permit to manipulate small scale magnets and use them as memory devices, or spin-wave emitters. The SP current can also stabilize configurations that are energy maxima. In this scenario, the free magnetization exhibits the phenomenology of the systems subjected to time-dependent driving forces [14]. This dynamic behaviors includes solitons, domain walls, and spatially periodic textures or *patterns*. Typical spin-transfer torque





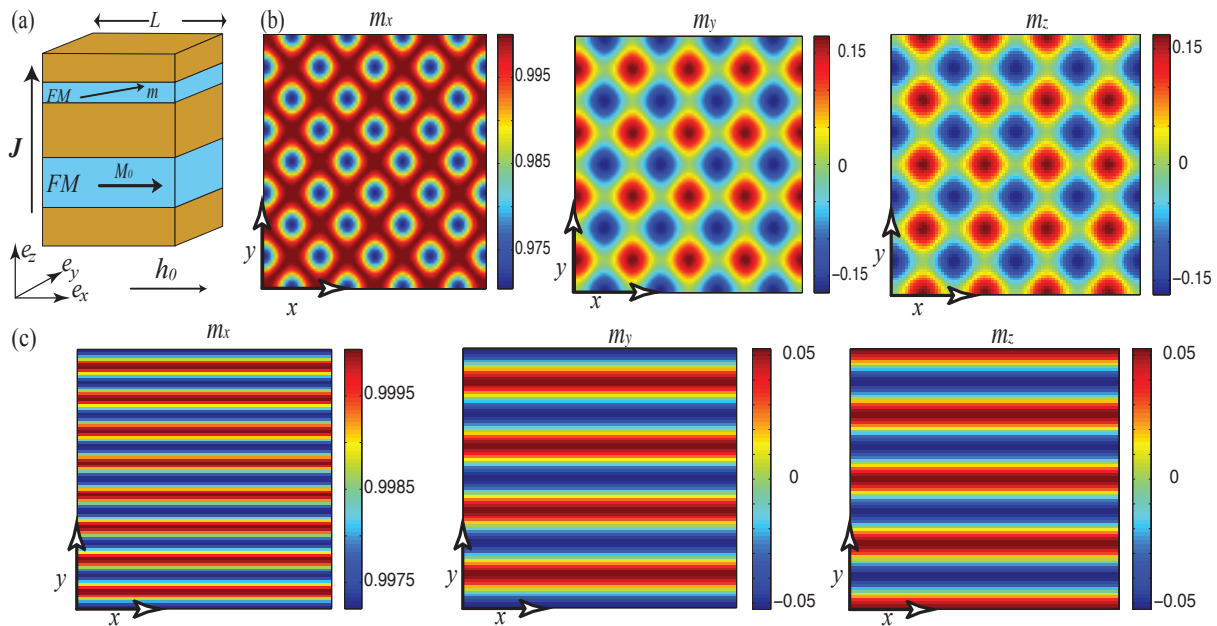


**Figure 1.** Nanopillar device and magnetic textures. a) Schematic spin-valve setup. The layers labeled as FM are the ferromagnets, the rest of the structure is composed by nonmagnetic conductors;  $J$  is the SP electric current while  $h_0$  is the external magnetic field, both effects are parallel to the easy-axes of the ferromagnetic layer under study.  $\mathbf{M}_0$  stands for the magnetization of the fixed layer. b) Typical patterns induced by the spin-transfer torque effect. The parameters are  $h_0 = -6$ ,  $g = -0.4999$ ,  $\beta_z = 1$ ,  $\beta_x = 0.5$ ,  $\alpha = 0.05$ , and  $dx = 0.126289$ . The parameters of the torque are  $\Delta = b = 0$ , this is the sinus-approximation case. c) The same as b) with the Slonczewski torque, it is,  $\Delta = 0$  and  $b = 0.35$ . Note the relation between the magnetic components  $m_y \approx -m_z$ . Since  $m_x \approx 1 - (m_y^2 + m_z^2)/2$ , the component  $m_x$  has spatial oscillations at twice the wavenumber of  $m_y$  and  $m_z$ .

induced patterns are shown in Figs. 1(b) and 1(c), they emerge due to an imbalance between the spin-polarized current and an external magnetic field [15]. The typical wavelength of these patterns is 20 – 30nm.

In the classical approach, the free layer magnetization is described by the Landau-Lifshitz-Gilbert equation with an extra term that accounts for the interaction between the spin-polarized electric current and the ferromagnet [3, 4, 5]. Since the transport of the conducting electrons depends on the relative orientations of the free and fixed layers, the torque induced by the SP current can also depend on this orientation. This dependence is known as the *angular dependence of the spin-transfer torque*. Analytic expressions for this angular dependence have been proposed and studied for several geometries [1, 16, 19, 17, 18, 20]. In certain regions of the parameter space, the dynamics of the precessional states change quantitatively and qualitatively with the use of different torque terms, which permits to test the angular dependence for a given geometry [17, 18, 21, 22]. The textures predicted in Refs. [14, 15] are an alternative dynamical regime which permits to compare the predictions of the different spin-transfer models. In Ref. [15], a simplified version of the torque was used, and a more general study is required.

The aim of this article is to study the role of the angular dependence of the spin-transfer torque in pattern formation. We obtain analytic solutions for the spatially periodic patterns and elucidate their stability. It is found that the magnetic textures change strongly with the angular dependence. The manuscript is organized as follows: in Sec. 2, we describe the magnetization



dynamics of the free layer. In Sec. 3, we obtain the amplitude equation for the patterns, and analyze the role of the angular dependence. The conclusions and remarks are left to the final section.

## 2. Free layer magnetization dynamics

Consider a square cross-section nanopillar device, with fixed layer magnetization  $\mathbf{M}_0$  along the positive  $x$ -axis, this material is thicker than the free layer, and acts as a spin filter or spin polarizer for the electric current. Lateral sizes  $L$  in the transverse directions are around 100 nanometers for typical devices. Hereafter, we adimensionalize the magnetization of the free layer  $\mathbf{M} \rightarrow M_s \mathbf{m}$  and the external field  $\mathbf{H}_0 \rightarrow M_s \mathbf{h}_0$  by the saturation magnetization  $M_s$ ; the time  $t \rightarrow \gamma M_s t$  is written in terms of the gyromagnetic constant  $\gamma$ , and  $M_s$ ; and the spatial coordinates  $(x, y) \rightarrow l_{\text{ex}}(x, y)$  in terms of the *exchange length*  $l_{\text{ex}} \equiv \sqrt{2A/(\mu_0 M_s^2)}$  where  $A$  is the exchange coupling in the ferromagnet. For example, in a  $3\text{nm}$  thick Cobalt layer,  $M_s \simeq 1.4 \cdot 10^6 \text{ A/m}$ , and the characteristic time and space scales are  $(\gamma M_s)^{-1} \simeq 3.2\text{ps}$  and  $l_{\text{ex}} \approx 3.4\text{nm}$ , respectively [5].

For thin films, the magnetic energy is given by [5]

$$E = \frac{\mu_0 M_s^2}{L^2} \int_0^L \int_0^L \left[ -\mathbf{m} \cdot \mathbf{h}_0 - \frac{1}{2} \beta_x m_x^2 + \frac{1}{2} \beta_z m_z^2 + \frac{1}{2} |\nabla \mathbf{m}|^2 \right] dx dy, \quad (1)$$

an external magnetic field  $\mathbf{h}_0 = h_0 \mathbf{e}_x$  points along the  $x$ -axis. The coefficients  $\beta_x$  and  $\beta_z$  are combinations of the anisotropy constants with respect to the appropriate axes, where  $\beta_x$  ( $\beta_z$ ) favors (disfavors) the free magnetization in the  $x$ -axis ( $z$ -axis). Since the free layer is thin, the demagnetization field can be approximated by a shape anisotropy, and it is incorporated in the  $\beta_z$  coefficient.

The dynamic of the free layer magnetization is modeled by the dimensionless Landau-Lifshitz-Gilbert equation (LLG) with an extra term that accounts for the spin-transfer torque [5]

$$\frac{\partial \mathbf{m}}{\partial t} = -\mathbf{m} \times \mathbf{h}_{\text{eff}} + \alpha \mathbf{m} \times \frac{\partial \mathbf{m}}{\partial t} + \eta g_0 \mathbf{m} \times (\mathbf{m} \times \mathbf{e}_x). \quad (2)$$

The first term of the right hand side of Eq. (2) accounts for the conservative precessions generated by the effective field,

$$\mathbf{h}_{\text{eff}} \equiv -\frac{L^2}{\mu_0 M_s^2} \frac{\delta E}{\delta \mathbf{m}} = (h_0 + \beta_x m_x) \mathbf{e}_x - \beta_z m_z \mathbf{e}_z + \nabla^2 \mathbf{m}. \quad (3)$$

The second and third terms of Eq. (2) are the phenomenological Gilbert damping and the spin-transfer torque, respectively. The dimensionless parameter  $g_0$  is

$$g_0 \equiv \frac{\hbar J}{2d|e|\mu_0 M_s^2}, \quad (4)$$

where  $J$  is the electric current density,  $d$  the thickness of the layer and  $e < 0$  the electric charge. The parameters  $J$  and  $g_0$  are negative when the electrons flow from the fixed to the free layer. The dimensionless function  $\eta = \eta(\mathbf{m} \cdot \mathbf{e}_x)$  is known as the spin-torque efficiency, this function depends on the relative orientation of the ferromagnetic films, and the device geometry and the physical properties of the layers, it has the general form of [4, 17, 18]

$$\eta(\mathbf{m} \cdot \mathbf{e}_x) \equiv \frac{(1 - b^2)}{1 - b + \Delta(1 + b)} \left( \frac{1}{1 + b m_x} + \frac{\Delta}{1 - b m_x} \right). \quad (5)$$



The coefficient  $\Delta$  measures the anisotropy between ferromagnetic layers of the spin-valve. In the case of an symmetric structure (identical ferromagnetic layers and leads)  $\Delta$  vanishes. Additionally, for short leads,  $\Delta$  can be neglected. In these cases, the efficiency is just  $\eta = (1 + b)/(1 + bm_x)$ , which is term originally proposed by Slonczewski [1, 16]. The constant  $b$  accounts for the strength of the spin scattering at the free layer interface. Notice that the  $\eta$  function is  $\eta(1) = 1$  in the parallel configuration. The approximation  $\eta(m_x) \approx \eta(1) = 1$  for  $m_x \approx 1$ , which is equivalent to impose  $b = 0$  in the formula (5), is known as the sinus spin-transfer torque, because the torque  $\|\eta g_0 \mathbf{m} \times (\mathbf{m} \times \mathbf{e}_x)\| \sim |\sin(\Psi)|$ , where  $\Psi$  is the angle between the free and fixed magnetizations. This approximation is widely used in literature. We will compare the SP-driven dynamics in the case of a general torque ( $b, \Delta > 0$ ), a symmetric torque ( $\Delta = 0$ ), and a sinus torque ( $b = 0$ ).

Notice that the LLG Eq. conserves the magnetization norm  $\|\mathbf{m}\| = 1$ , since  $\mathbf{m}$  and  $\partial_t \mathbf{m}$  are perpendicular. This permits us to use a spherical representation of the free magnetization

$$\mathbf{m} = \sin(\theta) [\cos(\phi)\mathbf{e}_x + \sin(\phi)\mathbf{e}_y] + \cos(\theta)\mathbf{e}_z. \quad (6)$$

Introducing this representation in Eq. (2), one obtains the following set of equations

$$\begin{aligned} \partial_\tau \theta &= -(h_0 + \alpha \eta g_0) \sin(\phi) + (\alpha h_0 - \eta g_0) \cos(\phi) \cos(\theta) + \frac{\alpha}{2} \sin(2\theta) [\beta_z + \beta_x \cos^2(\phi)] \\ &\quad - \frac{\beta_x}{2} \sin(\theta) \sin(2\phi) + \sin(\theta) \nabla^2 \phi + 2 \cos(\theta) \nabla \phi \cdot \nabla \theta + \alpha \nabla^2 \theta - \frac{\alpha}{2} \sin(2\theta) (\nabla \phi)^2, \\ \sin(\theta) \partial_\tau \phi &= (\eta g_0 - \alpha h_0) \sin(\phi) - (\alpha \eta g_0 + h_0) \cos(\phi) \cos(\theta) - \frac{1}{2} \sin(2\theta) [\beta_z + \beta_x \cos^2(\phi)] \\ &\quad - \alpha \frac{\beta_x}{2} \sin(\theta) \sin(2\phi) + \alpha \sin(\theta) \nabla^2 \phi + 2\alpha \cos(\theta) \nabla \phi \cdot \nabla \theta - \nabla^2 \theta + \frac{1}{2} \sin(2\theta) (\nabla \phi)^2, \end{aligned} \quad (7)$$

where  $\tau = t/(1 + \alpha^2)$ , and  $\eta = \eta(\sin(\theta) \cos(\phi))$ . The simplest equilibria of Eq. (2) are  $\mathbf{m} = \pm \mathbf{e}_x$ , which represent a free magnetization parallel (+) or anti-parallel (−) to the fixed magnetization  $\mathbf{M}_0$ . Both states correspond to extrema of the free energy  $E$ . In spherical coordinates, the parallel and anti-parallel states are  $(\theta, \phi) = (\pi/2, 0)$ , and  $(\theta, \phi) = (\pi/2, \pi)$  respectively. From the technological viewpoint, when both equilibria are stable, the spin-valve can be seen as a two-states system capable of saving information. Resistance measurements permit to read such data from the valve, and the spin-transfer torque induced switching allows one to write on the device. This is the basis of the spin-transfer torque based RAM memories [4].

For the rest of the manuscript we will concentrate on the parallel equilibrium  $\mathbf{m} = \mathbf{e}_x$ .

### 3. Periodic patterns

Note that the linear stability analysis around the  $m_x = 1$  state is independent of the parameters  $b$  and  $\Delta$  because the angular dependence is constant around the parallel state,  $\eta(m_x) = \eta(1) + \mathcal{O}(m_y^2 + m_z^2) \approx 1$ . The instabilities of this state have been subject of several studies the last decades [3, 4, 5, 15]. There are three main types of bifurcations: the Andronov-Hopf instability that generates self-oscillations, the stationary instability in which the system goes to other stationary equilibria, and the spatial instability (see Ref. [15] for more details); this last bifurcation is the motivation of the of this work. The spatial instability is characterized because the perturbations that destabilize the parallel state are non-uniform and generally give rise to periodic patterns. In the case of a spin-valve, when  $g_0, h_0 < 0$ , the SP current favors the parallel state while the external field disfavors it. The competition of these opposing effects is the physical origin of the spatial instability. Considering a critical perturbation of the form

$$\begin{pmatrix} \theta \\ \phi \end{pmatrix} \approx \begin{pmatrix} \pi/2 \\ 0 \end{pmatrix} + e^{\lambda t} [A_0 e^{i\mathbf{q}\cdot\mathbf{r}} + \bar{A}_0 e^{-i\mathbf{q}\cdot\mathbf{r}}] \begin{pmatrix} 1 \\ 1 \end{pmatrix}, \quad (8)$$



where the growth rate is  $\lambda = \beta_z/2 + g_0$ . The norm  $q$  of the wave-vector  $\mathbf{q}$  is controlled by the external magnetic field through  $q = -h_0 - \beta_x - \beta_z/2$ , and it exists for  $h_0 < -\beta_x - \beta_z/2 < 0$ . The complex amplitude  $A_0$  is a constant fixed by the initial conditions, and  $\bar{A}_0$  is the complex conjugate of  $A_0$ . The spatially periodic perturbations are amplified on time for  $g_0 > -\beta_z/2$ , or decay to zero for  $g_0 < -\beta_z/2$ . Notice that since the nanopillar has a square cross-section, there can be several admitted modes with wave-numbers  $q$ , which will grow and interact for  $g_0 > -\beta_z/2$ .

In the critical situation  $g_{0,c} \equiv -\beta_z/2$ , there is no exponential growth or decay of the perturbations, and the modes of formula (8) exhibit a slow dynamics given by the nonlinear corrections. At the onset of the spatial bifurcation, it is possible to obtain the equations for the critical modes by introducing the following ansatz

$$\begin{pmatrix} \theta \\ \phi \end{pmatrix} = \begin{pmatrix} \pi/2 \\ 0 \end{pmatrix} + [A(t)e^{iqx} + B(t)e^{iqy} + \bar{A}(t)e^{-iqx} + \bar{B}(t)e^{-iqy}] \begin{pmatrix} 1 \\ 1 \end{pmatrix} + \mathbf{W}(A, B, \bar{A}, \bar{B}, \mathbf{r}), \quad (9)$$

where the amplitudes  $A(t)$  and  $B(t)$  are slowly varying functions of time, and  $\mathbf{W}$  is a small correction that appears due to the nonlinear nature of the problem, and it depends nonlinearly on the amplitudes  $A$  and  $B$ . We have considered just two modes by the sake of simplicity, and the amplitudes  $A(t)$  and  $B(t)$  are the envelopes of the spatial oscillations along the  $x$ -axis and  $y$ -axis, respectively. Replacing the above ansatz in Eq. (7), linearizing in  $\mathbf{W}$ , and after imposing a solvability condition [23], we obtain

$$\begin{aligned} \frac{dA}{dt} &= (g_0 - g_{0,c})A - \Gamma A (|A|^2 + 2|B|^2), \\ \frac{dB}{dt} &= (g_0 - g_{0,c})B - \Gamma B (|B|^2 + 2|A|^2), \end{aligned} \quad (10)$$

where the coefficient of the nonlinearity is

$$\Gamma = \frac{3}{2} \frac{\beta_z b}{1 - b^2} \frac{(1 - b)^2 - \Delta(1 + b)^2}{1 - b + \Delta(1 + b)}. \quad (11)$$

The above set of equations describes the growth of the pattern for  $g_0 > g_{0,c}$ , with a nonlinear interaction between modes, and a nonlinear saturation (or nonlinear gain) for  $\Gamma > 0$  ( $\Gamma < 0$ ). Let us start with the case of a nonlinear saturation  $\Gamma > 0$ . Notice that the set of Eqs. (10) is phase invariant, it is, they remain unchanged under transformations of the form  $(A, B) \rightarrow (Ae^{i\psi_1}, Be^{i\psi_2})$  for arbitrary real constants  $\psi_1$  and  $\psi_2$ . This motivates the use of reduced real valued variables  $a_1(t) = \sqrt{\Gamma}|A(t)|$ , and  $a_2(t) = \sqrt{\Gamma}|B(t)|$  for the case of nonlinear saturation,

$$\begin{aligned} \frac{da_1}{dt} &= \epsilon a_1 - a_1 (a_1^2 + 2a_2^2), \\ \frac{da_2}{dt} &= \epsilon a_2 - a_2 (a_2^2 + 2a_1^2). \end{aligned} \quad (12)$$

where  $\epsilon \equiv g_0 - g_{0,c}$ . For negative  $\epsilon$ , the spatially periodic perturbations decay to the homogeneous solution  $(a_1, a_2) = (0, 0)$ , which is linearly stable. Hence, the parallel state is stabilized by the current for negative enough values of  $g_0$ .

Figure 2 shows the phase portrait of Eq. (12) for positive values of  $\epsilon$ . The 4 steady states of the system are the parallel state  $(a_1, a_2) = (0, 0)$ , the roll patterns  $(a_1, a_2) = (\sqrt{\epsilon}, 0)$  and  $(a_1, a_2) = (0, \sqrt{\epsilon})$ , and finally the square texture  $(a_1, a_2) = (\sqrt{\epsilon/3}, \sqrt{\epsilon/3})$ . Given the amplitude



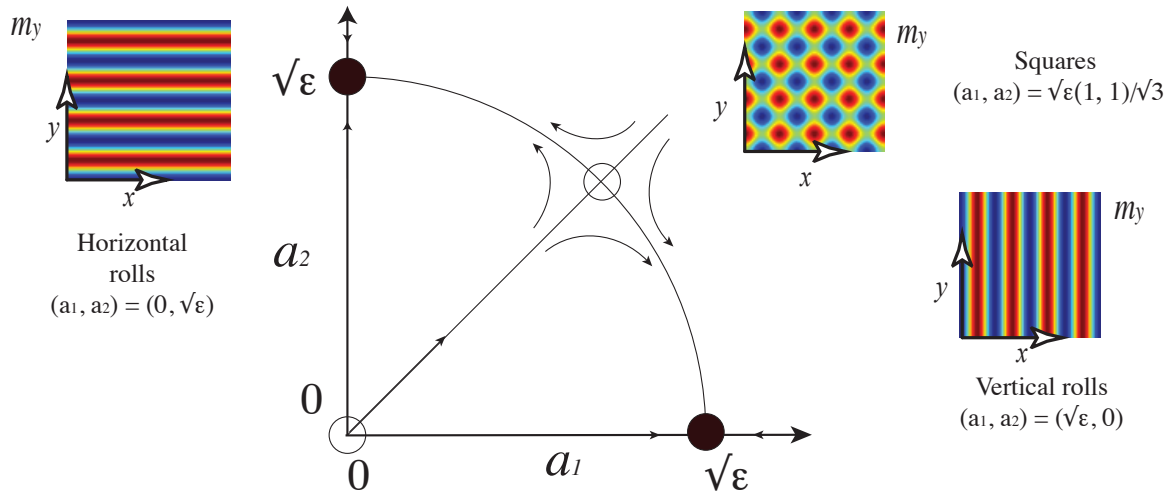


**Figure 2.** Phase portrait of amplitude Eq. (12), which describes the pattern formation driven by a Slonczewski spin-transfer torque. Insets show the magnetic component  $m_y$  of the equilibrium states. For  $g_0 > g_{0,c}$  the vertical and horizontal roll equilibria (black circles) are stable for the Slonczewski form of the torque. The Square pattern and the uniform solution (empty circles) are unstable.

Eq. (12), the linear stability analysis of the patterns becomes a trivial task. This analysis reveals that the roll states are stable (black circles in Fig. 2) and the square is unstable (empty circle). Thus, after transients, the magnetization converges to the horizontal or vertical rolls of the form

$$m_x \approx 1 - 4(g_0 - g_{0,c}) \left[ \frac{1 - b^2}{\beta_z b} \frac{1 - b + \Delta(1 + b)}{(1 - b)^2 - \Delta(1 + b)^2} \right] \left( \frac{1 - \cos(\mathbf{q} \cdot \mathbf{r})}{3} \right),$$

$$m_y \approx m_z \approx 2\sqrt{g_0 - g_{0,c}} \sqrt{\frac{2}{3} \frac{1 - b^2}{\beta_z b} \frac{1 - b + \Delta(1 + b)}{(1 - b)^2 - \Delta(1 + b)^2}} \cos(\mathbf{q} \cdot \mathbf{r}), \quad (13)$$

where  $\mathbf{q} \cdot \mathbf{r} = qx$  or  $\mathbf{q} \cdot \mathbf{r} = qy$ . Fig. 1(c) shows this state. This roll-like functions are the typical magnetic configurations for the most general spin-torque.

In the next subsections, we discuss the different types of instabilities that arise with each spin-transfer torque term. These transitions correspond to supercritical ( $\Gamma > 0$ ), quintic supercritical ( $\Gamma = 0$ ), and subcritical ( $\Gamma < 0$ ).

### 3.1. Slonczewski limit ( $\Gamma > 0$ )

If the spin-valve has equal ferromagnetic films and equal leads, then  $\Delta = 0$  and the  $\eta(m_x)$  function is the same as proposed originally by Slonczewski in Refs. [1, 16]. In this case, the saturation coefficient takes the form

$$\Gamma = \frac{3}{2} \frac{\beta_z b}{1 + b}. \quad (14)$$

Figure 1(c) illustrates the rolls for  $b = 0.35$ . This type of bifurcation is known as a supercritical transition. It is worth noting that the saturation is independent of the external field  $h_0$  and easy-axis anisotropy constant  $\beta_x$ . Figure 3(a) compares the numerical solution of the Landau-Lifshitz-Gilbert equation with the predicted amplitude  $2|A|(\epsilon) \sim 2(\epsilon/\Gamma)^{1/2}$  of rolls  $m_y \approx -m_z \approx 2|A| \cos(\mathbf{q} \cdot \mathbf{r})$ . In order to integrate the LLG equation, space was discretized using a finite differences centered scheme of order six, and the temporal evolution was obtained with a fifth order variable step size Runge-Kutta.



The magnetoresistance  $\delta r$  permits to compare predicted textures with experimental data. Hence, it is an adequate physical quantity for characterizing magnetic configurations in spin-valves. For uniform magnetized free layers, the magnetoresistance depends only on the relative orientation between the free and fixed layers,  $\delta r = \delta r(m_x)$ . For nonuniform magnetic states, the average indicator  $\delta r \equiv \delta r(m_x^{av})$  is commonly used [24], where  $m_x^{av}$  is the average magnetization along the  $x$ -axis. Consequently, for symmetric spin-valves the average resistance will be independent of external field and anisotropy coefficient  $\beta_x$ .

### 3.2. Sinus-approximation ( $\Gamma = 0$ )

In the sinus approximation ( $b = 0$ ), the function  $\eta$  is constant and the cubic coefficients of the set of Eqs. (10) vanishes. In order to quantify the saturation, it is necessary to include higher order corrections into the amplitude equation. This case was studied in detail in Ref. [15]. Let us summarize the main results of Ref. [15], and compare them with the predictions of other type of spin-transfer torques. In a similar way of the previous section, we consider a two modes ansatz of the form

$$\begin{pmatrix} \theta \\ \phi \end{pmatrix} \approx \begin{pmatrix} \pi/2 \\ 0 \end{pmatrix} + R [A(t)e^{i\mathbf{q}_1 \cdot \mathbf{r}} + B(t)e^{i\mathbf{q}_2 \cdot \mathbf{r}} + \bar{A}(t)e^{-i\mathbf{q}_1 \cdot \mathbf{r}} + \bar{B}(t)e^{-i\mathbf{q}_2 \cdot \mathbf{r}}] \begin{pmatrix} 1 \\ 1 \end{pmatrix} + \mathbf{W}'(A, B, \bar{A}, \bar{B}, \mathbf{r}), \quad (15)$$

where the wave-vectors  $\mathbf{q}_1$  and  $\mathbf{q}_2$  have norm  $q$ , and their orientation is fixed by the border of the sample. The prefactor  $R$  is the characteristic scale for patterns induced by a sinus torque, which is defined as

$$R \equiv \sqrt[4]{\frac{4\beta_z}{(6\beta_x + 3\beta_z - 2q^2)^2}}. \quad (16)$$

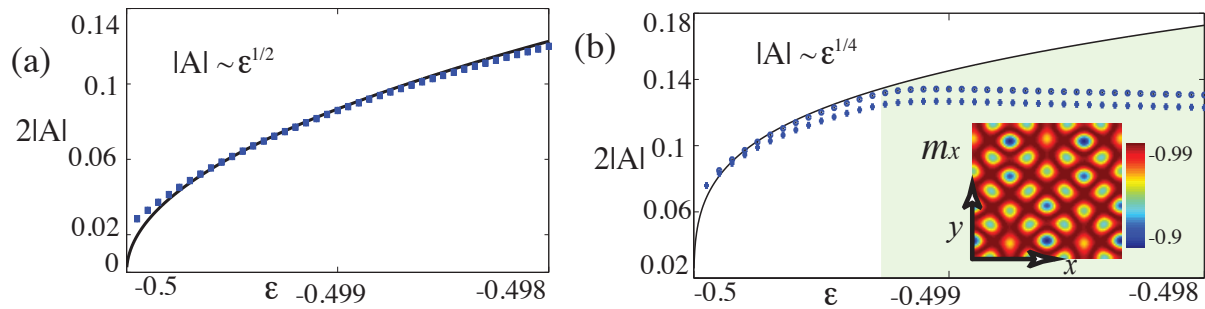


**Figure 3.** Comparison between analytic calculations (solid lines) and micromagnetic simulations (crosses and circles). (a) Pattern amplitudes for the Slonczewski spin-transfer torque with  $b = 0.55$ , and  $\Delta = 0$ . The solid line is the solution roll solutions of Eq. (10), while crosses + and circles • stand by the maximum of the Fourier transform of  $m_z$  and  $m_y$ , respectively. It is worth noting that at dominant order  $|m_y| \approx |m_z| \approx |\phi| \approx |\theta - \pi/2|$ . The fields  $(m_y, m_z)$  were obtained with the direct integration of the LLG Eq. (2) with  $h_0 = -6$ ,  $\beta_x = 0.5$ ,  $\beta_z = 1$ ,  $\alpha = 0.05$ , and spatial step size  $dx = 0.126289$ . (b) The same as in (a) for a sinus spin-transfer torque ( $b = 0$ ). At the onset of the spatial instability, the amplitudes of follow the law  $|A| \sim \epsilon^{1/4}$  predicted by the amplitude equation (17), nevertheless far from the bifurcation the square pattern becomes unstable giving rise to the stationary pattern of the inset.



Replacing the ansatz (15) in the LLG equation and imposing solvability condition, we get

$$\begin{aligned}\frac{dA}{dt} &= \epsilon A - \frac{8}{3} \frac{2-3D}{1-D} A|A|^2|B|^2 - A|A|^4 - \frac{8}{3} \frac{1}{1-D} A|B|^4, \\ \frac{dB}{dt} &= \epsilon B - \frac{8}{3} \frac{2-3D}{1-D} B|B|^2|A|^2 - B|B|^4 - \frac{8}{3} \frac{1}{1-D} B|A|^4,\end{aligned}\quad (17)$$

with  $\epsilon \equiv g_0 - g_{0,c}$ . Note that the modes interaction is mediated by quintic nonlinearities. This type of transition is known as quintic supercritical bifurcation. The parameter  $D$  accounts for the competition between the external magnetic field and the anisotropies

$$D \equiv \frac{2}{3} \frac{q^2}{2\beta_x + \beta_z} = \frac{2|h_0| - 2\beta_x - \beta_z}{6\beta_x + 3\beta_z}. \quad (18)$$

The above set of equations admits roll solutions of the form  $(|A|, |B|) = (\epsilon^{1/4}, 0)$  and  $(|A|, |B|) = (0, \epsilon^{1/4})$ . The phase portraits of the set of Eqs. (17) are shown in Fig. 4. These solutions are linearly stable when the field  $|h_0|$  is small compared with the anisotropy constants (or equivalently  $D < 1$ ). For intense fields ( $D > 1$ ) the rolls become unstable. In the last case, the square-like equilibrium  $A = B = (\epsilon/9)^{1/4}$  is linearly stable. Figure 1(c) shows a square pattern obtained for  $h_0 = -6$ , where  $D > 1$ . The phase portrait of this case is in Fig. 4(b). For the critical value of the external field  $h_{0,c} = -2(2\beta_x + \beta_z)$  the quintic saturation vanishes, and the analysis of pattern formation requires higher order corrections.

Since the saturation is given by the quintic order nonlinearities, then the equilibrium states grow as  $m_y \sim m_z \sim (g_0 - g_{0,c})^{1/4}$  as illustrated in Fig. 3(b). Moreover, the  $m_x$  magnetization component follows the law  $m_x \sim (g_0 - g_{0,c})^{1/2}$ . Note that the square pattern of Fig. 1(c) becomes unstable when  $g_0$  surpasses a critical value; in this situation additional modes grow and interact. In the context of dynamical systems this bifurcation is known as a secondary instability of the underlying pattern. A different pattern appears from this instability as shown in the inset of Fig. 3(b).

In brief, the case of the sinus approximation: the equilibrium magnetization depends on the external field and the anisotropies; there is a transition for a critical value of the external field, in this transition the roll solutions interchange stability with the square-like pattern. Finally, the magnetoresistance depends on the square-root of the current  $\delta r \sim (g_0 - g_{0,c})^{1/2}$ .

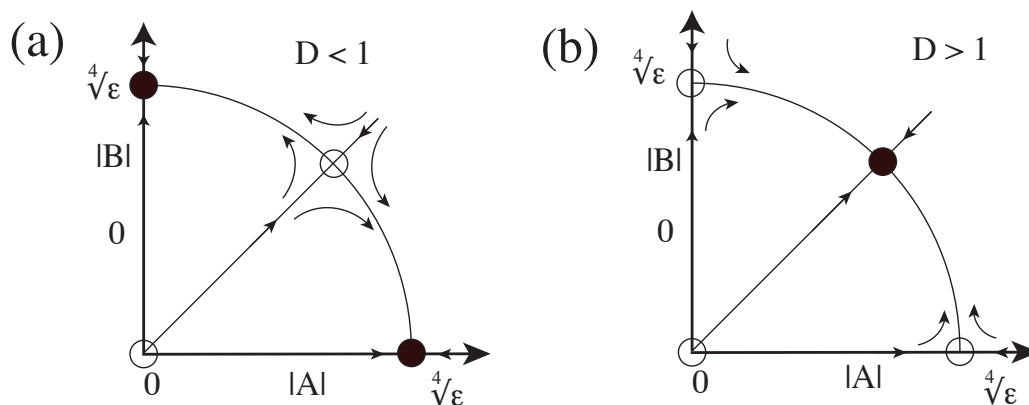


**Figure 4.** Phase portrait of amplitude Eq. (17), where a sinus-approximation for the spin-transfer torque has been considered. Black circles stand for stable pattern equilibria, while empty circles are for unstable states. a) Small external field ( $D < 1$ ) favors the formation of rolls. b) High external magnetic field ( $D > 1$ ) favors the square equilibrium.



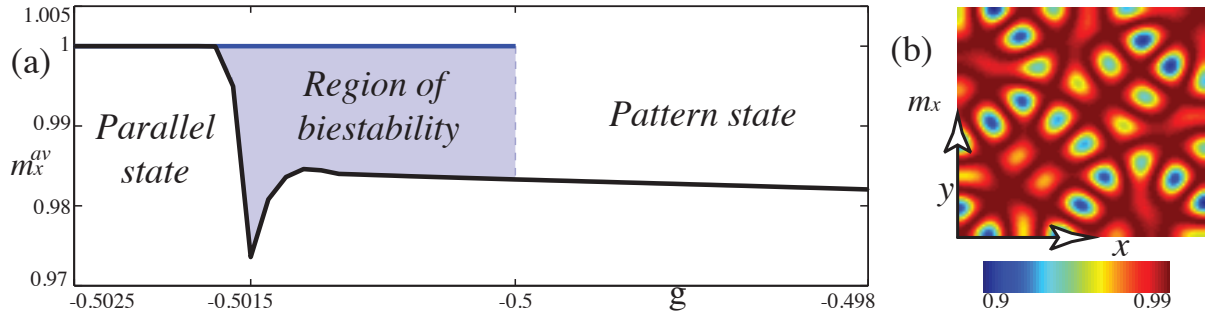


**Figure 5.** Hysteresis loop for asymmetric spin-valves. (a) The spatial average  $m_x^{av}$  of  $m_x$ , at equilibrium, is obtained integrating the LLG Eq. (2) with  $b = 0.55$ ,  $\Delta = 0.2$ ,  $h_0 = -6$ ,  $\beta_x = 0.5$ ,  $\beta_z = 1$ ,  $\alpha = 0.05$ , and spatial step size  $dx = 0.126289$ . (b)  $m_x$  component of the equilibrium magnetization for  $g_0 = g_{0,c}$ .

### 3.3. Hysteresis ( $\Gamma < 0$ )

A completely different scenario occurs for highly asymmetric spin-valves. If the coefficient  $\Delta$  surpasses the critical value  $\Delta_c = (1 - b)^2 / (1 + b)^2$ , the cubic nonlinearities amplify the pattern and higher order corrections must be included in Eq. (10). In such case the spatial instability is subcritical, and patterns exist even for  $g_0 < g_{0,c}$ . Physical systems with subcritical spatial instabilities are characterized by an hysteresis region close to the critical point (in this case  $g_0 = g_{0,c}$ ), it is, both the parallel state and patterns are stable. Figure 5 illustrate the hysteresis for the spatial average of the magnetization component  $m_x$  at equilibrium,  $m_x^{av}$ . Hence, in the case of asymmetric enough spin-valves, the magnetoresistance has a discontinuity.

From the viewpoint of dynamical systems, subcritical spatial instabilities generate a wide variety of states, such as domain walls, localized patterns, and interacting solitary structures [23], among others. The self-organization of highly asymmetric spin-valves forced with spin-polarized currents is an open problem, which could be interesting for memory technologies.

## 4. Conclusions and remarks

We have studied the formation of periodic textures in spin-valves, with a general type of spin-transfer torque. Using the weakly nonlinear analysis, we have found that the type of spatial instability changes from supercritical, to quintic supercritical and subcritical bifurcations depending on the form for the spin-transfer. The sinus approximation gives a pattern growing law of  $(g_0 - g_{0,c})^{1/4}$ , the magnetoresistance depends on the anisotropies and the external field. In opposition, for the Slonczewski spin-transfer torque and the general spin-transfer torque, the textures grow as  $(g_0 - g_{0,c})^{1/2}$ , and the magnetoresistance is independent of the external field and the easy-axis anisotropy  $\beta_x$ . Moreover, for highly asymmetric spin-valves, the spatial instability that creates patterns becomes subcritical, which generate hysteresis loops. Numerical simulations of the Landau-Lifshitz-Gilbert equation confirm these predictions. We expect that the formation of textures will permit to have an additional dynamical test to the spin-transfer torque terms, as well as possible application of pattern states in technology.

## Acknowledgments

I thank Marcel G. Clerc for fruitful discussions. I gratefully acknowledge financial support from Becas Conicyt 2012, Contract No. 21120878.

## References

- [1] Slonczewski J C, J. 1996 *Mag. Mat. Mag.* **159** L1.



- [2] Berger L 1996 *Phys. Rev. B* **54** 9353.
- [3] Ralph D C, and Stiles M D 2008 *J. Magn. Mag. Mater.* **320** 1190.
- [4] Stiles M D, and Miltat J, in *Spin Dynamics in Confined Magnetic Structures*, edited by B. Hillebrands, A. Thiaville (Springer, Berlin, 2006) Vol. 3, Chap. 7
- [5] Mayergoyz I D, Bertotti G, and Serpico C, *Nonlinear Magnetization Dynamics in Nanosystems* (Elsevier, Oxford, 2009).
- [6] Katine J A, Albert F J, Buhrman R A, Myers E B, and Ralph D C 2000 *Phys. Rev. Lett.* **84** 3149.
- [7] Kiselev S I, Sankey J C, Krivorotov I N, Emley N C, Schoelkopf R J, Buhrman R A, and Ralph D C 2003 *Nature (London)* **425** 380.
- [8] Kiselev S I, Sankey J C, Krivorotov I N, Emley N C, Rinkoski M, Perez C, Buhrman R A, and Ralph D C 2004 *Phys. Rev. Lett.* **93** 036601.
- [9] Kiselev S I, Sankey J C, Krivorotov I N, Emley N C, Garcia A G F, Buhrman R A, and Ralph D C 2005 *Phys. Rev. B* **72** 064430.
- [10] Lee K J, Deac A, Redon O, Nozieres J P, and Dieny B 2004 *Nature Materials* **3** 877.
- [11] Bertotti G, Serpico C, Mayergoyz I D, Magni A, d'Aquino M, and Bonin R 2005 *Phys. Rev. Lett.* **94** 127206.
- [12] Berkov D V, and Gorn N L 2008 *J. Phys. D* **41** 164013.
- [13] Slavin A, and Tiberkevich V 2009 *IEEE Trans. Magn.* **45** 1875.
- [14] León A O, and Clerc M G 2015 *Phys. Rev. B* **91** 014411.
- [15] León A O, Clerc M G, and Coulibaly S 2014 *Phys. Rev. E* **89** 022908.
- [16] Slonczewski J C 2002 *J. Mag. Mat. Mag.* **247** 324.
- [17] Xiao J, Zangwill A, and Stiles M D 2004 *Phys. Rev. B* **70** 172405.
- [18] Xiao J, Zangwill A, and Stiles M D 2005 *Phys. Rev. B* **72** 014446.
- [19] Xiao J, Zangwill A, and Stiles M D 2007 *Eur. Phys. J. B* **59** 415.
- [20] Barnas J, Fert A, Gmitra M, Weymann I, and Dugaev V K 2005 *Phys. Rev. B* **72** 024426.
- [21] Kim W, Lee S-W, and Lee K-J 2011 *J. Phys. D* **44** 384001.
- [22] Lee S-W, and Lee K-J 2010 *IEEE Trans. Magn.* **46** 2349.
- [23] Pismen L M *Patterns and Interfaces in Dissipative Dynamics*, (Springer Series in Synergetics, Berlin Heidelberg 2006).
- [24] Lee K J, Deac A, Redon O, Nozieres J P, and Dieny B 2004 *Nature Materials* **3** 877.